Investigating the transition from central peak to peak-ring basins using central feature volume measurements from the Global Lunar DTM 100 m

Veronica J. Bray,[1] Corwin Atwood-Stone,[1] and Alfred M. McEwen[1]

[1] Several theories have been suggested to explain the transition from peak to peak-ring crater morphology. In order to explore the transition and assess the currently advocated peak-ring formation theories, we have collected measurements of central feature volumes and heights for relatively fresh lunar impact craters. We employed the Global Lunar DTM 100 m, which has the vertical precision and spatial coverage necessary to accurately measure peak and peak-ring volumes in more craters than previously possible. The similarity in both trend and magnitude of peak and peak-ring volumes suggests that peak-ring formation is closely related to the development of central peaks as crater size increases. Our data thus lends support to those peak-ring formation theories involving peak collapse. **Citation:** Bray, V. J., C. Atwood-Stone, and A. M. McEwen (2012), Investigating the transition from central peak to peak-ring basins using central feature volume measurements from the Global Lunar DTM 100 m, *Geophys. Res. Lett.*, *39*, L21201, doi:10.1029/2012GL053693.

1. Introduction

[2] Above crater diameters of 140–170 km on the Moon, the most common internal feature is a peak-ring [e.g., *Hale and Grieve*, 1982]. Peak-rings are defined as concentric rings of rugged hills, peaks, and massifs that protrude from an otherwise flat crater floor, inside the crater rim [*Grieve et al.*, 1981]. Proto-basins - craters with both a central peak and peak-ring (Figure 1c) - are considered to be transitional crater-types between the central peak (Figure 1a) and peak-ring (Figure 1d) morphologies. Several contrasting theories explaining the transition from peak to peak-ring basins have been constructed using terrestrial structural data, theory, hydrocode simulations, and most commonly on the basis of crater morphology catalogs [e.g., *Pike*, 1977, 1980, 1985; *Wood and Head*, 1976; *Wilhelms et al.*, 1987; *Pike and Spudis*, 1987; *Hale and Head*, 1979; *Croft*, 1985; *Hartmann*, 1972]. These theories include: the collapse of an unstable central uplift [e.g., *Baldwin*, 1963; *Melosh*, 1982], the formation of nested craters [cf. *Quaide and Oberbeck*, 1968] due to differential depths of crater excavation in layers of contrasting strength [e.g., *Hodges and Wilhelms*, 1978], the formation of an exterior ring by mega-terracing [e.g., *Head*, 1974], and

as a result of the differential scaling of the melt and transient crater cavities [e.g., *Cintala and Grieve*, 1998].

[3] Two models of peak-ring formation are currently being strongly advocated – the hydrodynamic collapse of the central peak [*Morgan et al.*, 2000; *Collins et al.*, 2002] and the differential melt scaling model, which has been further developed and referred to as the nested melt cavity model [*Head*, 2010; *Baker et al.*, 2011]. Both models predict a crater diameter-dependent continuum of crater morphologies from peak to proto-basin to peak-ring, and are both supported by the observed increase in the ratio of peak-ring diameter and rim-to-rim diameter (Dpr/D) as crater diameter (D) increases [e.g., *Alexopoulos and McKinnon*, 1994; *Baker et al.*, 2011]. Volume measurements are an important additional measurement for distinguishing which of these theories is the most likely as, depending on the style of formation, the volume progression of the central features are likely to differ. Volume data is less common than diameter measurements, and thus has been used sparsely for assessment of peak-ring formation [*Hale and Grieve*, 1982]. We have extracted central feature volume measurements from the Global Lunar DTM 100 m [*Scholten et al.*, 2011b], and used these data to assess the currently advocated peak-ring formation theories.

1.1. Model Predictions

[4] The most broadly accepted peak-ring formation theory at present is that of central peak collapse [e.g., *Morgan et al.*, 2000; *Collins et al.*, 2002]. This theory requires a temporary weakening of the planetary surface during impact crater formation to allow an over-extended, gravitationally unstable central uplift to collapse in a fluid-like manner. This weakening increases with growing crater size, allowing the full collapse of central uplifts in large craters to form a peak-ring. Such size-dependent weakening is supported by measurement of crater wall slopes, which provide a proxy for the static coefficient of friction. The average wall slopes of lunar craters decrease as crater diameter increases [*Pike*, 1976], demonstrating a progressive effective weakening of the target material during impact as crater size increases.

[5] Peak collapse theory predicts that the height and diameter (and therefore volume) of a central uplift will increase until just prior to peak-ring formation, at which point the peak collapses, decreasing relative peak heights and increasing peak diameter as peak material is redistributed. Depending on how much of the peak base spreads below the floor melt lens, the measured volume of central peaks is expected to be conserved as the peak-ring transition is approached. As peak-rings are formed from peak material, in this model, the volume of peak-rings is predicted to show some relationship to the volume of central peaks. As with peak development, the observed volume of these peak-rings

[1]Lunar and Planetary Laboratory, Tucson, Arizona, USA.

Corresponding author: V. J. Bray, Lunar and Planetary Laboratory, 1541 E University Blvd., Tucson, AZ 85721, USA. (vjbray@lpl.arizona.edu)
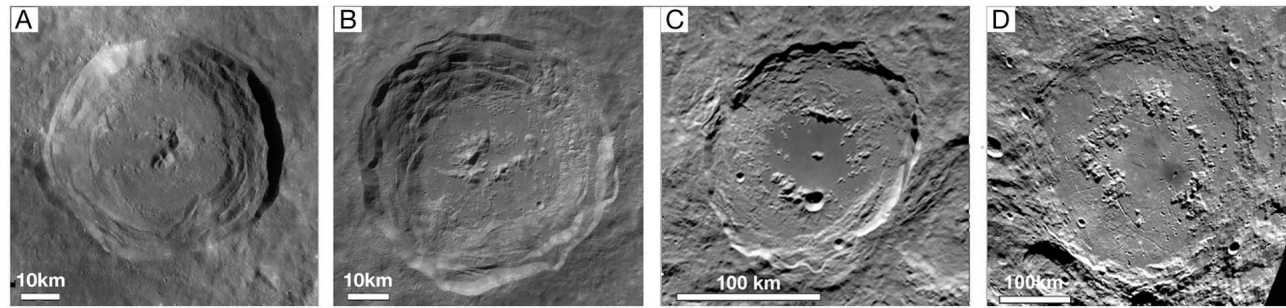
Figure 1. Images of the four morphological types noted in this work, North is up in all images: (a) Maunder, a 54 km diameter central peak crater, (b) Zucchius a 63 km ringed peak crater, (c) Antoniadi, a 138 km diameter proto-basin with large peak and small peak-ring, (d) Schrodinger, a 320 km diameter peak-ring crater.

might be obscured somewhat by rising melt levels within the crater.

[6] A theory that is receiving increased attention of late is that of the nested melt cavity model [e.g., *Head*, 2010; *Baker et al.*, 2011]. The differential growth of the crater cavity and melt volume as impactor size increases results in disproportionately more melt being produced in larger impact events. Central peak craters are hypothesized to form from uplift during a relatively melt-poor "uplift-dominated" regime. As crater diameter increases the relative amount of melt increases impeding the uplift until only the edges of the melt cavity can uplift, forming a peak-ring surrounding the central melt pool.

[7] The nested melt cavity theory predicts an unrelated progression in central feature dimensions. In small complex craters, peak size will increase with growing crater size. Prior to the peak-ring transition, both peak height and diameter are predicted to decrease as the amount of central uplift becomes subdued by the larger melt cavity. The theory therefore predicts a decrease in peak volumes prior to the peak-ring transition at crater diameters of ~140 km. As peak-rings are created through uplift of the solid edges of the melt cavity, peak-ring formation is not directly connected to peak development, and thus peak-ring volumes will not necessarily show any trend continuation or relation to peak volumes.

1.2. The GLD100

[8] The Global Lunar DTM 100 m (GLD100) [*Scholten et al.*, 2011b] was created from over 44,000 LROC WAC stereo images, tied to LOLA data [*Smith et al.*, 2010]. The combined product has a pixel spacing of 100 m, a vertical accuracy of 10–30 m, and is 99.84% complete between 80°N and 80°S (lighting conditions reduce DTM accuracy at higher latitudes). A comparison with LOLA data has determined that the mean difference between GLD100 and LOLA heights is only 4 m, and the 1-σ RMS error is 23 m, i.e., less than one-third of a WAC pixel (75 m) [*Scholten et al.*, 2011a]. The added benefit of the GLD100 is the relative lack of data gores, compared to LOLA's limited cross-track coverage away from the poles. The GLD100 has the vertical precision and spatial coverage necessary to accurately measure peak and peak-ring volumes, in more craters than previously possible. An additional advance since the volume measurements of (e.g.) *Croft* [1978] and *Hale and Grieve* [1982] is the existence of improved image processing tools (e.g., ArcMap). These now allow feature volumes to be directly measured from the DTM, rather than via calculation from 2D

topographic profiles, thus reducing errors/inaccuracies and lessening the effect of natural variation in crater shape with azimuth.

2. Method

[9] We collected measurements from 62 fresh central peak and 'ring-like central peak' craters, three proto-basins and six peak-ring craters (Figure 1). Freshness was judged based on the crater rim, wall scallops and central feature being crisp and well defined; floor melt deposits and wall/peak material are obviously separate units (an indicator of the freshest craters) [cf. *Pohn and Offield*, 1970; *Head*, 1975]. These constraints were relaxed somewhat for the larger crater sizes as un-degraded peak-ring basins are rare. All craters included in this work have depth-diameter ratios in line with that defined for fresh craters by *Pike* [1976]. Each crater used in this work and its surrounding area were cropped from the 100 m resolution Lunar Reconnaissance Orbiter Camera (LROC) Wide Angle Camera (WAC) Global Mosaic [*Robinson et al.*, 2010], and from the GLD100 [*Scholten et al.*, 2011b]. For collection of central feature elevations and volumes, the cropped DTM and image of each crater was entered into ArcMap (www.esri.com).

[10] Central feature height was measured from the crater floor to the tip of the peak or the highest elevation of the peak-ring (H_{cf}, Figure 2c). The peak-to-terrain elevation (PTE) of a fresh crater provides an alternative measure of the uplift height. PTE is unaffected by variable floor melt sheet thickness, or other factors that obscure the base of the central uplift, and would thus decrease the central feature height measurement. As the surrounding terrain level is highly variable around most craters, the peak-to-terrain elevation was measured from the highest elevation of the central feature to the *average* terrain elevation beyond the crater rim and ejecta blanket, as measured from 8 cross sectional profiles through the crater.

[11] To allow the most accurate calculation of exposed central feature volume possible, the base of the central feature was defined as a variable slope, rather than assuming a uniform plain. To generate this sloped base, the crater floor surrounding the central feature was selected (Figure S1C) and the Terrain Slope tool of ArcMap used to predict the most likely basal topography (Figure S1D). The volume of the central feature above this base was then computed by integrating beneath the DTM, down to the sloped base. The horizontal extent of the peak or peak-ring was defined
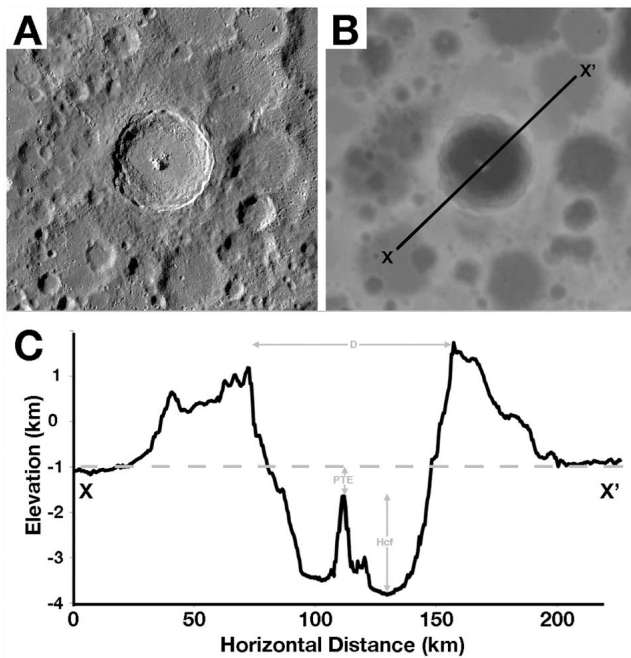
Figure 2. (a) LRO WAC image of Tycho crater (43S:11W), (b) Tycho area of the GLD100. One of eight cross-sectional profiles was extracted from the GLD100 along the line X to X′. (c) The resultant topographic profile. The average terrain level beyond the ejecta blanket is marked with a dashed grey line. Peak to terrain elevation was measured from the highest peak point measured on any of the 8 profiles, to the average surrounding terrain level.

by inspection of the WAC image and the GLD100. Any positive/negative relief features within the central feature that were not related to the main crater were removed manually when necessary to prevent a later-forming crater, for example, from affecting central feature volume. Diameters measured from the GLD100 have a measurement error of ±100 m, heights are accurate to ±30 m. The largest uncertainty in the volume estimate was due to how the limits of the peak are defined by the user. Reproducibility tests show a 5% variation on peak volumes when measured multiple times by different workers.

3. Results

[12] Central feature volume increases as crater diameter increases (Figure 3a). The data used for this figure can be found in Table S1 in the auxiliary material.[1] *Hale and Grieve* [1982] noted a decrease in the rate of central peak volume increase at crater diameters between 50 and 80 km. We also note two distinct trends in central peak volume above and below crater diameters of ~80 km. The technique employed by *Hale and Grieve* [1982] did not take account of variation in the crater floor elevation - volumes were calculated above a fixed elevation level. As the volume measurements presented here incorporated the sloped base of central features (Figure S1), some deviation between the two datasets is understandable.

[13] The central feature volumes of peak-ring and proto-basins follow the same trend as that of central peaks in craters above 80 km in diameter ($V_{cf} = 0.0005D^{2.74}$, $R^2 = 0.85$). No increase or decrease in central feature volume is notable across the transition from peaks to peak-rings at crater diameters of 140–170 km.

[14] Central feature height as measured from the crater floor, and as inferred from the peak to terrain elevation measurement, are presented in Figures 3b and 3c, respectively. Both are presented in order to highlight any differences between peak and peak-ring height. Relative central peak height (H_{cp}/D, Figure 3b) decreases with crater size after crater diameters of ~100 km according to: $H_{cp}/D = 6.74\ D^{-1.20}$ ($R^2 = 0.78$). Proto-basin and peak-ring craters follow this decreasing trend and therefore contain relatively low-lying central features compared with those in the smaller central peak craters. However, normalized peak-to-terrain elevation (PTE/D, Figure 3c) values indicate that the peak-ring height relative to the surrounding terrain is no less than that of central peaks in craters of similar size. PTE/D of central peak craters decreases as crater size increases until crater diameters of approximately 80 km, at which point apparent uplift height becomes more variable. At crater diameters above 100 km the elevation of central features approaches the elevation of the surrounding terrain. After this elevation is reached, neither peaks nor peak-rings significantly decrease or increase in uplift amount and peak-rings are shown to have an uplift height no less than that of central peaks.

4. Discussion

[15] The increasing trend in central peak volumes is consistent with both peak-ring formation models considered here. A decrease in the rate of uplift volume occurs at D ~ 50–80 km. The decrease in central feature volume could be due to a relative decrease in the amount of crater floor uplift, the beginnings of peak collapse, or due to an increase in the amount of material obscuring the base of an otherwise unchanged degree of central uplift. As a decrease in actual uplift height (as inferred from peak-to-terrain elevation, Figure 3c) also occurs at D ~ 80 km it suggests that the volume decrease represents an actual decrease in the amount of central uplift, rather than the uplift base being obscured. This change does not immediately precede the peak to peak-ring transition and so may not be the volume decrease hypothesized by the nested melt cavity model. Instead, the trend in central feature volume is conserved approaching and across the peak to peak-ring transition, suggesting that while peak height is reducing relative to crater diameter, broader peak bases act to maintain the central feature volume. The continued trend in peak volumes prior to the peak-ring transition at D = 140–170 km better supports the peak collapse model of ring formation as central feature volume is predicted to be conserved.

[16] The contrast of PTE/D and H_{cf}/D trends suggests that the subtle decrease in peak-ring height relative to central peaks shown in Figure 3b is most likely due to increasing melt or debris fill of the crater floor – obscuring some of the peak-ring from view and thus reducing our H_{cf} and volume measurements from what would be considered the 'true' uplift height/volume. It is therefore probable that our recorded peak-ring volumes, being from craters that are
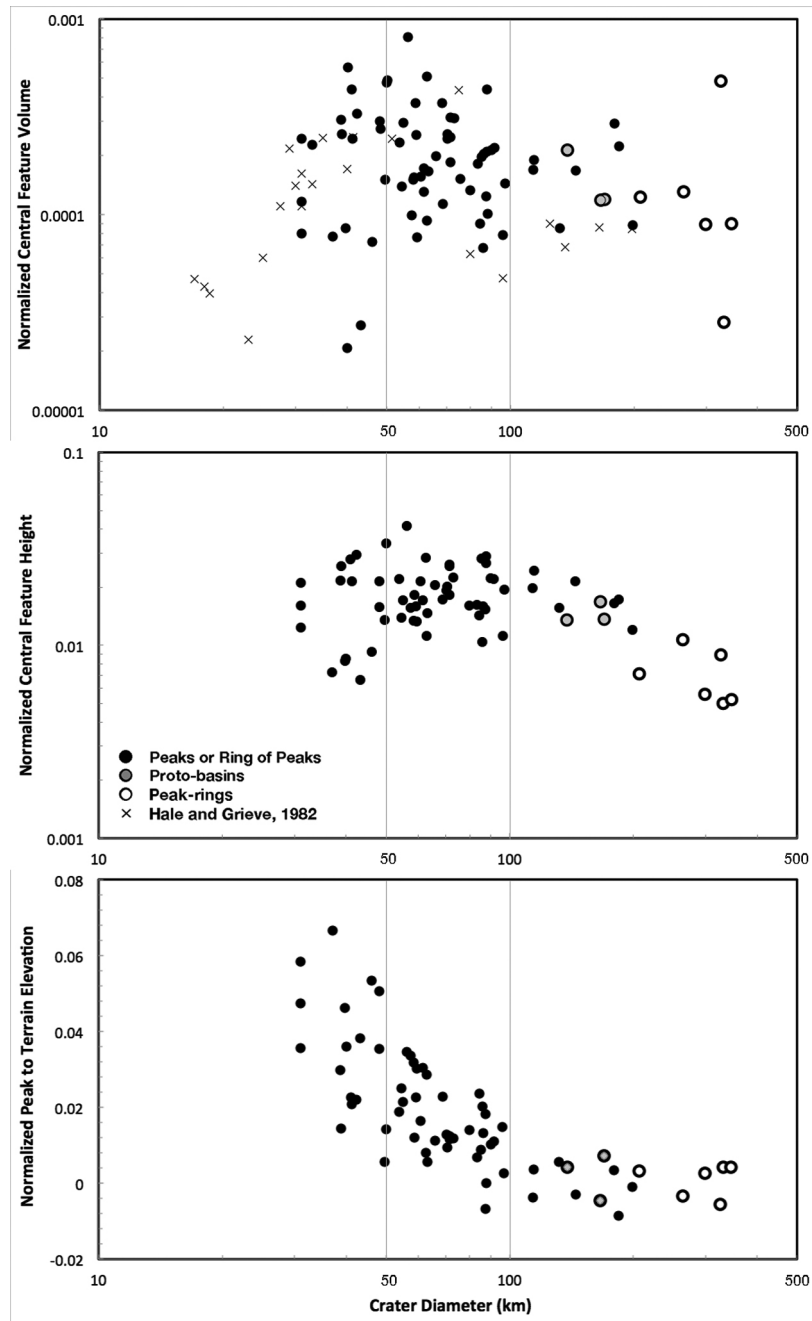
Figure 3. Crater dimensions relative to rim-to-rim diameter (D). (a) Normalized central feature volumes (V_{cf}/D^3). (b) Normalized central feature height as measured from the crater floor (H_{cf}/D). (c) Normalized peak-to-terrain elevation (PTE/D).

inherently more degraded and melt-filled than smaller examples, represent a lower bound volume obtained by measurement of the exposed portion of an uplift part-obscured by significant melt sheet thickness.

[17] The similarity in both trend and magnitude of peak and peak-ring volumes suggests that peak-ring formation is closely related to the development of central peaks. Our data thus lends support to those peak-ring formation theories that involve peak collapse.

References

Alexopoulos, J. S., and W. B. McKinnon (1994), Large impact craters and basins on Venus, with implications for ring mechanics on the terrestrial planets, in *Large Meteorite Impacts and Planetary Evolution*, edited by B. O. Dressler, R. A. F. Grieve, and V. L. Sharpton, *Spec. Pap. Geol. Soc. Am.*, *293*, 29–50.

Baldwin, R. B. (1963), *The Measure of the Moon*, Univ. of Chicago Press, Chicago, Ill.

Baker, D. M. H., J. W. Head, C. I. Fassett, S. J. Kadish, D. E. Smith, M. T. Zuber, and G. A. Neumann (2011), The transition from complex crater to peak-ring basin on the Moon: New observations from the Lunar Orbiter

Laser Altimeter (LOLA) instrument, *Icarus*, *214*, 377–393, doi:10.1016/j.icarus.2011.05.030.

Cintala, M. J., and R. A. F. Grieve (1998), Scaling impact-melt and crater dimensions: Implications for the lunar cratering record, *Meteorit. Planet. Sci.*, *33*, 889–912, doi:10.1111/j.1945-5100.1998.tb01695.x.

Collins, G. S., H. J. Melosh, J. V. Morgan, and M. R. Warner (2002), Hydrocode simulations of Chicxulub crater collapse and peak ring formation, *Icarus*, *157*, 24–33, doi:10.1006/icar.2002.6822.

Croft, S. K. (1978), Lunar crater volumes: Interpretation by model of impact cratering and upper crustal structure, *Proc. Lunar Planet. Sci. Conf.*, *9th*, 3711–3733.

Croft, S. K. (1985), The scaling of complex craters, *Proc. Lunar. Planet. Sci. Conf. 13th*, Part 2, *J. Geophys. Res.*, *90*, suppl., C828–C842.

Grieve, R. A. F., P. B. Robertson, and M. R. Dence (1981), Constraints on the formation of ring impact structures, based on terrestrial data, in *Multi-ring Basins, Proc. Lunar Planet. Sci.*, vol. 12, part A, edited by P. H. Schultz and R. B. Merrill, pp. 37–57, Pergamon, New York.

Hale, W. S., and J. W. Head (1979), Lunar central peak basins: Morphology and morphometry in the crater to basin transition zone, in *Reports of Planetary Geology Program, 1978–1979, NASA Tech. Memo., 80339*, 160–162, NASA, Wash. D.C.

Hale, W., and R. A. F. Grieve (1982), Volumetric analysis of complex lunar craters: Implications for basin ring formation, *Proc. Lunar Planet. Sci. Conf. 13th*, Part 1, *J. Geophys. Res.*, *87*, suppl., A65–A76, doi:10.1029/JB087iS01p00A65.

Hartmann, W. K. (1972), Interplanet variations in scale of crater morphology—Earth, Mars, Moon, *Icarus*, *17*, 707–713, doi:10.1016/0019-1035(72)90036-X.

Head, J. W. (1974), Orientale multi-ringed basin interior and implications for the petrogenesis of lunar highland samples, *Moon*, *11*, 327–356, doi:10.1007/BF00589168.

Head, J. W. (1975), Processes of lunar crater degradation: Changes in style with geologic time, *Earth Moon Planets*, *12*, 299–329, doi:10.1007/BF02629699.

Head, J. W. (2010), Transition from complex craters to multi-ringed basins on terrestrial planetary bodies: Scale-dependent role of the expanding melt cavity and progressive interaction with the displaced zone, *Geophys. Res. Lett.*, *37*, L02203, doi:10.1029/2009GL041790.

Hodges, C. A., and D. E. Wilhelms (1978), Formation of lunar basin rings, *Icarus*, *34*(2), 294–323, doi:10.1016/0019-1035(78)90169-0.

Melosh, H. J. (1982), A schematic model of crater modification by gravity, *J. Geophys. Res.*, *87*, 371–380, doi:10.1029/JB087iB01p00371.

Morgan, J. V., M. R. Warner, G. S. Collins, H. J. Melosh, and G. L. Christenson (2000), Peak-ring formation in large impact craters: Geophysical constraints from Chicxulub, *Earth Planet. Sci. Lett.*, *183*, 347–354, doi:10.1016/S0012-821X(00)00307-1.

Quaide, W. L., and V. R. Oberbeck (1968), Thickness determinations of the lunar surface layer from lunar impact craters, *J. Geophys. Res.*, *73*(16), 5247–5270, doi:10.1029/JB073i016p05247.

Pike, R. J. (1976), Crater dimensions from Apollo data and supplemental sources, *Moon*, *15*, 463–477, doi:10.1007/BF00562253.

Pike, R. J. (1977), Size-dependence in the shape of fresh impact craters on the moon, in *Impact and Explosion Cratering*, edited by D. J. Roddy, R. O. Pepin, and R. B. Merill, pp. 489–509, Pergamon, New York.

Pike, R. J. (1980), Formation of complex impact craters: Mars, *Icarus*, *43*, 1–19, doi:10.1016/0019-1035(80)90083-4.

Pike, R. J. (1985), Some morphologic systematics of complex impact structures, *Meteoritics*, *20*, 49–68, doi:10.1111/j.1945-5100.1985.tb00846.x.

Pike, R. J., and P. D. Spudis (1987), Basin-ring spacing on the Moon, Mercury, and Mars, *Earth Moon Planets*, *39*, 129–194, doi:10.1007/BF00054060.

Pohn, H. A., and T. W. Offield (1970), Lunar crater morphology and relative age determination of lunar geologic units—Part 2. Applications, *U.S. Geol. Surv. Prof. Pap.*, *700-C*, C163–C169.

Robinson, M. S., et al. (2010), Lunar Reconnaissance Orbiter Camera (LROC) instrument overview, *Space Sci. Rev.*, *150*, 81–124, doi:10.1007/s11214-010-9634-2.

Scholten, et al. (2011a), Complementary LRO global lunar topography datasets—A comparison of 100 meter raster DTMs from LROC WAC stereo (GLD100) and LOLA altimetry data, *Lunar Planet. Sci. Conf.*, *XXXXII*, Abstract 2080.

Scholten, F., J. Oberst, K. D. Matz, T. Roatsch, M. Wählisch, M. S. Robinson, and L. Team (2011b), GLD100—The global lunar 100 meter raster DTM from LROC WAC stereo models, *Lunar Planet. Sci. Conf.*, *XXXXII*, Abstract 2046.

Smith, D. E., et al. (2010), The Lunar Orbiter Laser Altimeter investigation on the Lunar Reconnaissance Orbiter mission, *Space Sci. Rev.*, *150*, 209–241, doi:10.1007/s11214-009-9512-y.

Wilhelms, D. E., J. F. McCauley, and N. J. Trask (1987), The geologic history of the Moon, *U.S. Geol. Surv. Prof. Pap.*, *1348*, 302 pp.

Wood, C., and J. Head (1976), Comparisons of impact basins on Mercury, Mars and the Moon, *Proc. Lunar Sci. Conf.*, *7th*, 3629–3651.